

Automatic Detection of UXO Magnetic Anomalies Using Extended Euler Deconvolution

Kristofer Davis*, Yaoguo Li, and Misac Nabighian

Center for Gravity, Electrical, and Magnetic Studies, Department of Geophysics, Colorado School of Mines

Summary

The paper presents an algorithm for automatic detection of UXO anomalies in total-field magnetic data based on the concept of structural index (SI) of a magnetic anomaly. The magnetic field produced by a dipole-like source, such as a UXO, varies with inverse distance cubed and therefore has an SI of 3. Identifying magnetic anomalies having structural indices of 3 enables direct detection of potential UXO targets. The recently developed Hilbert based extended Euler deconvolution method (Nabighian and Hansen, 2001) provides an efficient means for calculating the SI and enables use to perform automatic anomaly based on computed SI.

Introduction

Magnetometry has emerged as one of the most efficient and cost-effective methods for discriminating UXO targets. Recent work by Billings et al. (2002) has demonstrated that low false-alarm rates and a high degree of detection can be achieved through the inversion of static magnetic data objects. Successful application to large areas of such inversion-based discrimination algorithms depends on the ability to automatically detect targets by picking the anomalies that are caused by UXO-like objects. The commonly used method for anomaly picking has predominantly been the thresholding of total gradient data (often mistakenly referred to as the analytical signal). Billings and Herrmann (2003) introduced an automatic wavelet detection technique based on continuous wavelet transform using natural wavelets.

In this paper, we develop an alternative method for anomaly detection using the Hilbert transform based extended Euler deconvolution technique (Nabighian and Hansen, 2001). The method estimates both location and, more importantly, the type of magnetic source that produced the anomaly. Any anomaly whose source appears to be dipolar is considered a potential UXO target based on the assumption that the majority of UXO as well as small metallic objects act as magnetic dipoles.

Automatic detection by extended Euler deconvolution

Extended Euler deconvolution. The Euler deconvolution was originally developed in exploration geophysics for rapidly estimating the location and depth to magnetic or gravity sources. It is based on the fact that the potential

field produced by some sources obeys Euler's homogeneity equation. A given component of the magnetic anomalous field $B_a(x, y, z)$ satisfies:

$$B_a(tx, ty, tz) = t^n B_a(x, y, z), \quad (1)$$

where n is the degree of homogeneity. Carrying out simple differentiation, it can be shown from eq. (1) that,

$$x \frac{\partial B_a}{\partial x} + y \frac{\partial B_a}{\partial y} + z \frac{\partial B_a}{\partial z} = n B_a, \quad (2)$$

where x , y and z are the field coordinates and the source is assumed to be at the origin of coordinates. Equation (2) is known as Euler's homogeneity equation or simply Euler's equation. The degree of homogeneity characterizes how fast the field decreases as function of distance to the source and is dependent on source types. For example, the magnetic field produced by a dipolar source decreases as inverse distance cubed and the corresponding degree of homogeneity is $n = -3$.

Eq.(2) can be used to estimate the source depth from magnetic data in 3D, which gives rise to the method of Euler deconvolution (e.g., Reid et al. 1990). Since the potential field decreases inversely proportional with distance raised to some power, the degree of homogeneity is non-positive. The negative of the degree of homogeneity is defined as the structural index N .

Assuming that a compact source is located at (x_0, y_0, z_0) and the data are observed at (x, y, z) , we rewrite equation (2) as:

$$(x - x_0) \frac{\partial B_a}{\partial x} + (y - y_0) \frac{\partial B_a}{\partial y} + (z - z_0) \frac{\partial B_a}{\partial z} = -N B_a, \quad (3)$$

which is satisfied at each data point on the surface. Equation (3) contains four unknowns: x_0 , y_0 , z_0 and N . The x , y , z derivatives can be calculated using different algorithm depending on the distribution of original data. Applying equation (3) to a number of neighboring data points and, assuming an a priori value for N , we obtain a system of equations that can be solved in least squares sense for the source location (x_0, y_0, z_0) . The algorithm is usually applied to points within a window of a specified size.

The a priori choice of structural index has been the topic of much discussion in the literature since it is somewhat arbitrary and the obtained solutions depended strongly on its

Automatic detection of UXO magnetic anomalies

choice. Recent work by Nabighian and Hansen (2001) showed that the same Euler equation holds true also for the two components of 3D Hilbert transforms of the field:

$$\begin{aligned} (x-x_0)\frac{\partial H_x(B_a)}{\partial x} + (y-y_0)\frac{\partial H_x(B_a)}{\partial y} + (z-z_0)\frac{\partial H_x(B_a)}{\partial z} &= -NH_x(B_a), \\ (x-x_0)\frac{\partial H_y(B_a)}{\partial x} + (y-y_0)\frac{\partial H_y(B_a)}{\partial y} + (z-z_0)\frac{\partial H_y(B_a)}{\partial z} &= -NH_y(B_a), \end{aligned} \quad (4)$$

where H_x and H_y denote respectively the x- and y-component of the 3D Hilbert transform (Nabighian, 1984). Equation (4) in contrast with equation (3) does not require a background value since the Hilbert transform of a constant is equal to zero. Equations (3) and (4) together provide three Euler equations for a given set of magnetic data. As a result, we can carry out Euler deconvolution by using any one of, or combination of, the three equations. This leads to a more stable and versatile method of depth estimation. In particular, due to the absence of a background term in equations (4), one can use only these two equations and solve also for the structural index N . Thus we have an effective means to estimate not only the source location and depth but also its structural index.

Automatic anomaly detection. The ability to estimate the structural index and not specify it in advance means that we can distinguish between different source types during the depth estimation process. This enables us to identify UXO responses among the interfering anomalies of geologic origin. The majority of UXO items are predominantly dipolar sources. The corresponding total-field magnetic anomaly ΔT , is given by,

$$\Delta T(\mathbf{r}) = \frac{\mu_0}{4\pi} \mathbf{m} \cdot \nabla \nabla \frac{1}{|\mathbf{r}_0 - \mathbf{r}|} \cdot \hat{\mathbf{B}}_0, \quad (5)$$

where \mathbf{m} is the dipole moment, $\hat{\mathbf{B}}_0$ is a unit vector along the direction of ambient magnetic field, and \mathbf{r}_0 and \mathbf{r} are respectively the location of the dipole and observation points. Given the second order derivative applied to the inverse distance between source and observation points, it follows that the structural index of a dipolar field is 3.

The majority of geologic features tend to have some elongation and their magnetic anomalies would have a structural index less than 3. Based on this observation, we have developed a method for automatically picking UXO anomalies using calculated structural indices. The

central premise of the proposed method is that any compact source identified by Hilbert based extended Euler deconvolution as having a structural index close to 3 can be considered a potential UXO target and merits further investigation.

Equations (4) are applied throughout the entire data set within a sliding window. Each window yields a valid solution if there is a significant magnetic anomaly within that window. The reliability of a solution is often affected by the choice of window size, since a small window may not capture the anomaly pattern necessary for the calculation, and a large window may introduce interference from adjacent anomalies. For our application, we have chosen to use in succession multiple window sizes to allow for the variable depths of UXO targets in an area.

The method first performs a sequence of Hilbert based Euler deconvolution using different window sizes on the data set to obtain estimates of source depth and structural index. It then examines the variation of SI with window size and identifies the Euler solutions that yield SI values close to 3. Any anomalies with an SI close to 3, within a user specified tolerance, are treated as a potential UXO target.

Assuming a gridded magnetic data set ΔT , the details of the detection method is listed below:

Step-1: Compute the two horizontal derivatives, $\partial\Delta T/\partial x$ and $\partial\Delta T/\partial y$, using stabilized numerical differentiation operators in order to reduce noise.

Step-2: Compute the vertical derivative $\partial\Delta T/\partial z$ in the Fourier domain through the use of 3D Hilbert transform relations (Nabighian, 1984),

$$\begin{aligned} \Delta\tilde{T}_z &= \tilde{H}_x\Delta\tilde{T}_x + \tilde{H}_y\Delta\tilde{T}_y, \\ &\equiv -\frac{i\omega_x}{\sqrt{\omega_x^2 + \omega_y^2}}\Delta\tilde{T}_x - \frac{i\omega_y}{\sqrt{\omega_x^2 + \omega_y^2}}\Delta\tilde{T}_y, \end{aligned} \quad (6)$$

where ω_x and ω_y are the wavenumbers of 2D Fourier transform in the x- and y-direction, and $\Delta\tilde{T}_x$, $\Delta\tilde{T}_y$, and $\Delta\tilde{T}_z$ are respectively the Fourier transforms of the X, Y and Z derivatives of the total-field anomaly.

Step-3: Compute the two components of 3D Hilbert transform of the original total-field anomaly and their three spatial derivatives to obtain the eight quantities related to the magnetic field required in equation (4). The derivatives of each Hilbert transform component in (4) are obtained by applying Hilbert transform to the corresponding derivatives of the original total-field anomaly calculated in Steps 1 and 2.

Automatic detection of UXO magnetic anomalies

Step-4: Using the eight quantities calculated in Step-3 solve equation (4) in each window using least squares. A range of window sizes is used. This step yields both the x , y , z source location estimates and the structural index value N for that source.

Step-5: For the set of windows centered at the same location, find one solution whose structural index N is closest to 3. This solution is taken as the best solution associated with the set of windows located on a common center.

Step-6: If a solution exists and the structural index is greater than a threshold value, we assume that the algorithm has detected a possible UXO-like anomaly. The corresponding location provides a first order estimate for the dipole position.

Performing this procedure on a data set produces a map of detected anomalies and their source locations. The horizontal locations can be used subsequently to help extract individual anomalies for determining source parameters through dipole inversion.

Examples

To illustrate the method, we apply it to a synthetic and a field data set. The synthetic data were generated from 20 dipoles with random location, orientation, depth, and dipole moment. The depths range from 0.3 m to 0.8 m, with dipole inclinations and declinations ranging between -90° and 90° , and with dipole moments varying between 0.1 and 0.5 Am². The ambient field is assumed to have an inclination of 65° and declination of 25° .

We have applied our detection algorithm to this data set with window sizes varying between 3 to 25 grid points. Corresponding to each magnetic anomaly, a large number of Euler solutions were generated from windows that capture a reasonable part of the anomaly. The solutions in such a group differ only slightly from each other. Assuming all solutions within 0.1-m radius come from the same target, we clustered the solutions for the entire data set into 21 distinct anomalies. All detected anomalies have an SI greater than 2.5. Of these 21 solutions, 19 coincide with true anomalies in the data set, while two are located between adjacent anomalies. Thus, we have correctly detected 19 out of 20 anomalies, and produced two false alarms. The result is shown in Figure 1. We post the detection result over the color contour of magnetic anomaly. We note that the missed anomaly was a magnetic high located beside a negative anomaly. This confused the detection algorithm that placed a source between these two anomalies. The second false anomaly occurred between two closely spaced anomalies. This

solution was produced from a large window size that had difficulties recognizing the presence of two neighboring anomalies since the Euler solution assumes only one source per window.

The estimated horizontal locations of the 19 correctly detected anomalies agree well with the true locations. Furthermore, the estimated depths are also in agreement. The estimated dipole locations, therefore, provide a good first estimate for subsequent quantitative analyses.

As the second example, we apply the detection algorithm to the total-field data collected by the Army Corps of Engineers at the calibration grid at the Yuma proving ground in Yuma, AZ. The observed data are displayed in Figure 2. Numerous compact anomalies can be seen in the data plot.

We use window sizes varying from 3 to 25 grid points. The algorithm has identified the majority of the anomalies that are visible by visual inspection of the magnetic data. The Euler deconvolution solutions, however, are much more variable than those in the synthetic case. For example, the recovered structural indexes range from 1.0 to 3 instead of being close to 3. The reasons are twofold. First, some of the objects are rather large and buried at shallow depths. As a result, these anomalies do not behave exactly as dipole fields. Secondly, the response from geologic background is interfering with UXO responses. Hence their magnetic field decreases slower than inverse distance cubed. Consequently, the ideal scenario of a UXO anomaly having an SI of 3 no longer holds true. However, we have observed that thresholding the solution to retain those having $SI \geq 2$ enables us to detect the majority of UXO anomalies in this data set. Decreasing the threshold to a value less than two does not improve the detection capability, but produces a large number of false anomalies.

Using a threshold level of $SI = 2$, we have winnowed the solutions from Hilbert based extended Euler deconvolution, and clustered the retained solutions by grouping and averaging them within a 0.3-m radius as the final detection result. These are shown in Figure 3. The majority of the anomalies that are visible in the data are detected successfully. The result is consistent with that from the synthetic example in that overlapping anomalies, either between UXO responses or between UXO and some geologic response, tend to degrade the Euler solutions and cause false positives and false negatives. However, the overall detection result is successful to a large extent and the method is a promising candidate as an automatic detection algorithm in UXO clearance.

Discussion

We have developed an automatic anomaly detection algorithm by utilizing the Hilbert-based extended Euler

Automatic detection of UXO magnetic anomalies

deconvolution. Application to both synthetic and field data sets have demonstrated that the majority of buried UXO targets can be detected in total-field magnetic data. However, smaller separations between UXO targets do affect calculations based on single target detection within the window area. Presence of background geologic anomalies will also influence the solution as expected. Overall, the algorithm is expected to provide an alternative to much needed anomaly detection methods so that large data sets can be processed automatically. The corresponding estimates of locations and depths of detected anomalies will provide a reliable initial guess for subsequent quantitative inversion used in discrimination.

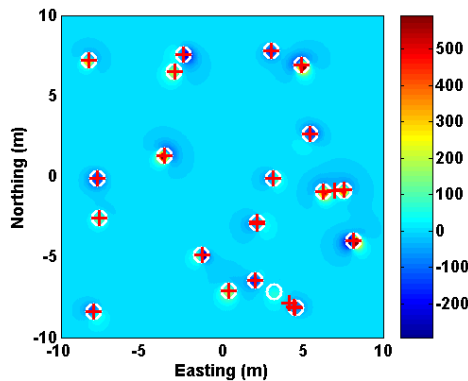


Figure 1. Result of automatic detection applied to synthetic total-field anomalies (nT) produced by 20 dipolar sources. The inducing field direction is $I=65^\circ$ and $D=25^\circ$. The “+” symbols indicate the source positions of the detected anomalies. For reference, the white ‘o’ symbols indicate the true dipole positions.

Acknowledgements

We thank Don Yule and Stephen Billings for helpful discussions on the topic. We also thank Don Yule and ERDC for supplying the YPG data. This research was supported by a grant provided by ERDC.

References

Billings, S. D., Pasion, L. R., and Oldenburg, D.W., 2002, UXO discrimination and identification using magnetometry, Proceedings of SAGEEP.

Billings, S. D. and Herrmann, F., 2003, Automatic detection of position and depth of potential UXO using a continuous wavelet transform., in Proceedings of SPIE Vol 5089, Detection and Remediation Technologies for

Mines and Mine like Targets VII, edited by Russell S. Harmon, John H. Holloway, J.T. Broach, pp 1012-1022.

Nabighian, M.N., 1984, Toward a three-dimensional automatic interpretation of potential field data via generalized Hilbert transforms: Fundamental relations: Geophysics, **49**, 780-786.

Nabighian, M. N., and Hansen, R. O., 2001, Unification of Euler and Werner deconvolution in three dimensions via the generalized Hilbert transform: Geophysics, **66**, 1805-1810.

Reid, A. B., J. M. Allsop, H. Granser, A. J. Millett, and I. W. Somerton, 1990, Magnetic interpretation in three dimensions using Euler deconvolution, Geophysics, **55**, 80-91.

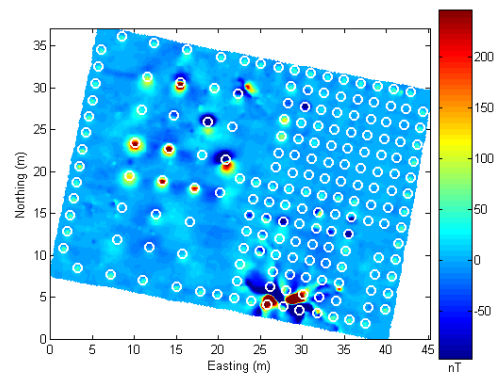


Figure 2. Total-field magnetic data collected at the calibration grid at Yuma Proving Ground in Yuma, AZ. The circles indicated the locations of emplaced objects.

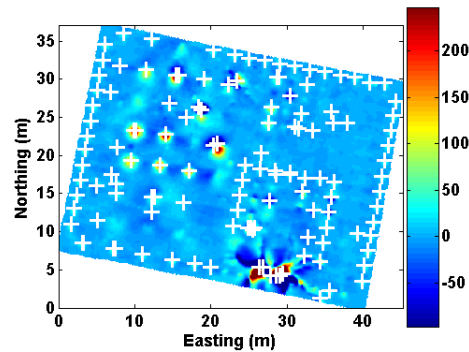


Figure 3. Result of automatic detection applied to total-field data (nT) from calibration grid at YPG, AZ. The threshold for SI is 2.0. The original solutions from the extended Euler deconvolution have been clustered by grouping and averaging those within a 0.3-m radius.